CAVITATION EVENT RATES AND NUCLEI DISTRIBUTIONS

Z. Liu, Y. Kuhn de Chizelle, and C. E. Brennen
California Institute of Technology
Pasadena, California

ABSTRACT

This paper examines the relationship between the cavitation event rates on axisymmetric headforms and the nuclei distributions in the incident flow. An analytical model is developed to relate these quantities and the results are compared with experimental cavitation event rates measured in the Large Cavitation Channel (LCC) at David Taylor Research Center (DTRC) on three different sizes of Schiebe body. The experiments were carried out at various cavitation numbers, tunnel velocities and air contents.

Boundary layer, bubble screening and observable cavitation bubble size effects on the event rates are examined. The trends in the event rates with changing cavitation number and body size are consistent with those observed experimentally. However the magnitudes of the event rates are about an order of magnitude larger than the experimental data. Nevertheless it is shown that the cavitation inception values predicted using a certain critical event rate are consistent with those observed experimentally.

Nomenclature

C	=Nuclei concentration
C_P	=Coefficient of pressure, $(p-p_\infty)/\frac{1}{2}\rho U^2$
C_{PM}	=Minimum C_P on a given streamline
C_{PMS}	=Minimum value of C_P on the headform surface
D	=Headform diameter
E	=Cavitation event rate
$N(R)$	=Nuclei density distribution function
R	=Radius of a cavitation nucleus
R_M	=Minimum radius of an observable cavitation bubble
R_C	=Critical cavitation nucleus radius
R_{max}	=Maximum cavitation bubble radius
S	=Surface tension
U	=Upstream tunnel velocity
U_M	=Maximum velocity corresponding to C_{PMS}
f_1, f_2, f_3	=Numerical factors effecting the cavitation event rate
p	=Fluid pressure
p_∞	=Pressure upstream
p_v	=Vapor pressure
r_H	=Headform radius
r_K	=Radius of curvature of streamlines near minimum pressure point
r_S	=Radius of minimum pressure point
r, y	=Normal distances of a given streamline from axis far upstream and from body surface near the minimum pressure point
s, s_0	=Coordinate along a streamline and the location of minimum pressure point
t_G	=Time available for bubble growth
u, u_M	=Fluid velocity, fluid velocity just outside boundary layer
v	=Velocity of a bubble normal to streamline
ρ	=Fluid density
σ	=Cavitation number, $(p_\infty-p_v)/\frac{1}{2}\rho U^2$
σ_{crt}	=Threshold cavitation number
σ_i	=Inception cavitation number
ξ, λ	=Factors in the chosen analytical expression for $N(R)$
ν	=Kinematic viscosity of fluid
μ	=Fluid viscosity
δ, δ_2	=Thickness and momentum thickness of boundary layer
ϵ	=Displacement of a bubble normal to streamline
Σ	=Function defined by equation (15).
Σ'	$=d\Sigma/d(r/r_H)$

1 Introduction

It has long been recognized that traveling bubble cavitation occurs as a result of micro-sized cavitation "nuclei" being convected into and then out of the low pressure regions in a flow. One consequence of this is the recognition that cavitation inception depends on the criterion one establishes in terms of the number of events per unit time. Because of the difficulties experienced in measuring the nu-

clei in a water tunnel (see Billet, 1985), there have been relatively few attempts to experimentally verify a relationship between the nuclei population in the incoming flow and the observed event rates. Two of the earliest attempts were the efforts by Ooi (1985) and Franklin and McMillan (1984) to synthesize the cavitation event rate in a submerged, turbulent jet (see also Pauchet *et al.*, 1992). However, one of the major uncertainties in that flow is the difficulty in characterizing the turbulent pressure fluctuations experienced by the bubble.

More recently Meyer *et al.* (1989,1992) have presented a theoretical model connecting the cavitation event rate on an axisymmetric headform with the nuclei distribution in the incident stream. The approximate analytical model presented by Ceccio and Brennen (1992) is similar in concept. The present paper refines this analytical model and adds the effects of the boundary layer, of bubble screening and of the finite size of the cavitation bubbles. Though more approximate than the numerical computations of Meyer *et al.* (1989, 1992), the analytical expressions provide insights into the important mechanisms and allow application in more complex flow geometries.

2 Experiments

The data presented in this paper was taken during tests conducted in the Large Cavitation Channel of the David Taylor Research Center in Memphis, Tennessee. Three geometrically similar axisymmetric headforms (Schiebe headform shape, Schiebe, 1972) measuring 5.08 cm, 25.4 cm and 50.8 cm in diameter were installed on the centerline of the tunnel and cavitation tests were conducted over a range of tunnel speeds (9 m/sec to 15 m/sec) and air contents (30% to 100% saturation at atmospheric pressure). The experimental arrangements are described elsewhere in greater detail (Kuhn de Chizelle *et al.*, 1992a,b) and will not be repeated here. It is sufficient to indicate that a large number of still photographs and a substantial quantity of video was taken for each operating condition (the video was synchronized to a strobe light to improve resolution).

Figure 1 presents the observed cavitation inception numbers, σ_i, as a function of headform diameter, D, tunnel velocity, U, and air-content relative to saturation at atmospheric pressure. Inception was based on an event rate of 50 cavitation events per second. Events were detected by means of flush-mounted electrodes, the current from which was modulated by the presence of a bubble (Ceccio and Brennen, 1992). The trends in figure 1 are fairly clear. The inception number increases with increasing headform size and the curves may well asymptote to the value of $(-C_{PMS})$. This headform size effect is simply a consequence of the fact that the larger the headform, the more nuclei are available for

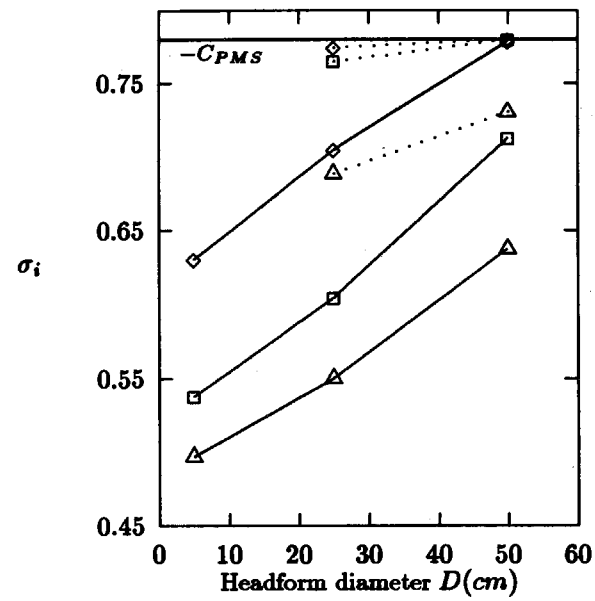

Figure 1: Experimentally observed cavitation inception numbers (based on 50 events/sec) as a function of tunnel velocity, headform size and air content. Velocity: 9 m/sec (◇), 11.5 m/sec (□) and 15 m/sec (△). Air content: 30% (——) and 80% (···)

cavitation and, therefore, for a specific event rate the value of σ_i will be larger. The values of σ_i also increase with increase in air content for a similar reason, namely more nuclei at the larger air contents. Figure 1 also demonstrates that the cavitation inception number increases with decreasing tunnel velocity. This effect is not so readily explained. However it is clear that to achieve the same cavitation number at a lower velocity one requires a higher tunnel pressure and it may be that the nuclei concentration in the tunnel increases considerably with decreasing operating pressure. We shall discuss this and other effects later in the paper.

3 Event Rate Observations

Both the photographs and the video tapes were analyzed in order to explore the variations in the cavitation event rates with headform size and tunnel velocity. The event rates were evaluated by counting the number of individual bubbles (or events) observable in a single frame and averaging this number over many frames. This allowed construction of figure 2 in which the average number of observable events is plotted against cavitation number, σ, for each of three velocities (9, 11.5 and 15 m/sec) for the three head-

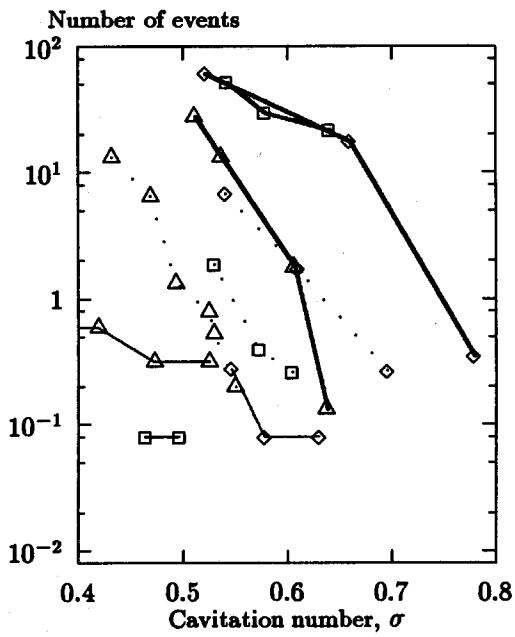

Figure 2: Average number of events observed on the headforms at an instant in time as a function of cavitation number, headform size and tunnel velocity. Velocity: 9 m/sec ($\diamond$), 11.5 m/sec ($\square$) and 15 m/sec ($\triangle$). Headform diameters: 5 cm (——), 25 cm (···) and 50 cm (——)

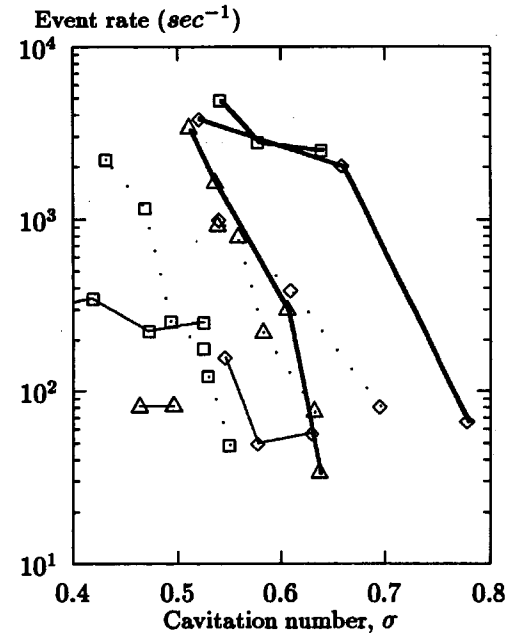

Figure 3: Cavitation event rates derived from figure 2 as a function of cavitation number, headform size and tunnel velocity. Velocity: 9 m/sec ($\diamond$), 11.5 m/sec ($\square$) and 15 m/sec ($\triangle$). Headform diameters: 5 cm (——), 25 cm (···) and 50 cm (——)

forms (this data is for 30% air content and we shall focus our attention on these conditions). Not surprisingly the number of events increases with decreasing cavitation number and with increasing headform size. Not so predictable is the tendency for the number of events to decrease with increasing speed but further comment on this effect is delayed until later.

The data on the number of events may be converted to cavitation event rates using bubble lifetimes obtained from knowledge of the velocity ($U_M = U(1 - C_{PMS})^{\frac{1}{2}}$ with C_{PMS} =-0.78) and the measured locations of bubble appearance and collapse as a function of σ (see Kuhn de Chizelle *et al.*, 1992a,b). The resulting event rate data for 30% air content is presented in figure 3 and it is clear that this is consistent with the cavitation inception data of figure 1 given the selected criterion of 50 events/sec.

As previously stated, one of the purposes of the present paper is to demonstrate the connection between the event rate (and by implication the inception number) and the nuclei number distribution. Before embarking on the details of this connection it is instructive to present the event rate data of figure 3 in the following modified form. Let us estimate that all the nuclei which pass through an annular stream tube bounded on the inside by the headform and on the outside by the stream surface which just touches the $C_P = -\sigma$ isobar (see figure 6) cavitate and therefore form observable bubbles. Then, using the potential flow velocity in this stream tube (therefore neglecting boundary layer effects) and using the data of figure 5 to estimate the thickness of the stream tube at each cavitation number, we can calculate the volume flow rate of liquid in the cavitating stream tube for each operating condition. Dividing the data of figure 3 by these values we obtain an estimate of the number of cavitation nuclei per unit liquid volume; this data is presented in figure 4. It is significant that some of the variation with cavitation number, headform size and tunnel velocity which was present in figures 2 and 3 has now been removed. Indeed, a large fraction of the data of figures 2 and 3 would appear to correspond to a nuclei concentration of the order of 0.1 nuclei/cm^3. The most noticeable deviation from this uniform value occurs at the highest speed (15 m/sec) with the two larger headforms.

The fact that a large fraction of the data appears to correspond to a similar nuclei concentration is simultaneously encouraging and puzzling. It is encouraging because it suggests that a more careful analysis which begins with the same nuclei number distribution and follows each nucleus along its streamline may allow synthesis of the event rates

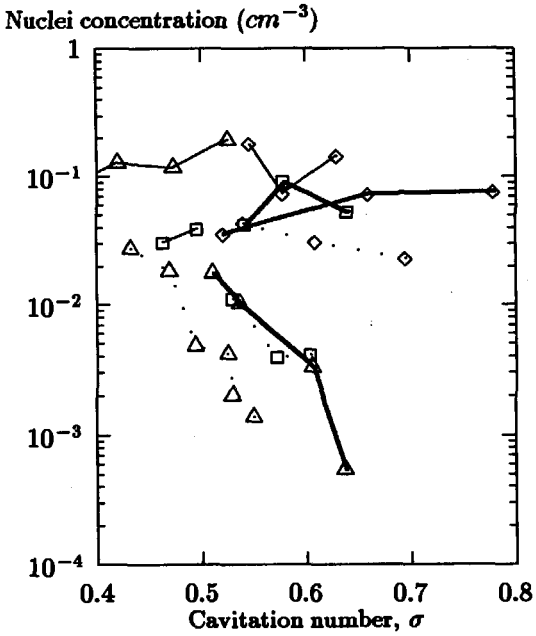

Figure 4: Effective concentrations derived from figure 3 as a function of cavitation number, headform size and tunnel velocity. Velocity: 9 m/sec (◇), 11.5 m/sec (□) and 15 m/sec (△). Headform diameters: 5 cm (——), 25 cm (···) and 50 cm (▬)

and the inception numbers. But it is also puzzling because the concentration of 0.1 nuclei/cm^3 is at least an order of magnitude smaller than most of the measurements of cavitation nuclei would suggest.

Referring to Billet's (1985) useful review of the subject of nuclei concentrations and distributions we note that the most reliable observations of nuclei (microbubbles and particles) have been obtained by systematically surveying the reconstructed holograms of volumes of tunnel water taken while the tunnel is in operation (for example, Gates *et al.*, 1978, 1979). For de-aerated tunnel water, such inspections typically reveal concentrations more than 20 nuclei/cm^3 with sizes ranging from about 5μm to about 200μm (see also Kato, 1990). However the next question to ask is what fraction of these potential nuclei do, in fact, cavitate when subjected to sub-critical pressures. Here the answer is quite unclear. The other principal method for counting nuclei is the cavitation susceptibility meter in which the liquid is drawn through an orifice (or other device) and therefore is subjected to low pressures. The device is of sufficiently small size so that cavitation events occur individually. Then the concentration of potential cavitation nuclei (as opposed to potential nuclei) is obtained from the measured event rate and the known volume flow rate. Billet's review indicates that the typical concentrations measured by susceptibility meters are usually of the order of 2 nuclei/cm^3, significantly smaller than the concentrations obtained by holographic methods. While this may suggest that only a fraction of the potential nuclei actually cavitate, the data is, as yet, inadequate to support any firm conclusion and may, of course, differ significantly from facility to facility. However, insofar as the present experiments are concerned, it is clear that actual cavitation nuclei concentrations are normally much larger than 0.1 nuclei/cm^3. This suggests that some other mechanism comes into play to produce such a small event rate on the present headforms.

4 Analytical Model for Cavitation Event Rate

A simple synthesis of the cavitation event rate from the nuclei distribution in the on-coming stream was presented by Ceccio and Brennen (1992). Here we explore this relationship further and comment on other factors which could significantly effect the event rate. We will use a nuclei number distribution function, $N(R)$, defined such that, per unit volume, the number of nuclei with radii between R and $R + dR$ is given by $N(R)dR$. From the measurement of free stream nuclei distribution in our laboratory (see Liu *et al.*, 1993), a characteristic form for $N(R)$ is

$$N(R) = C\frac{\log e}{(2\pi)^{1/2}\,\lambda R} exp(-\frac{(\log R - \log \xi)^2}{2\lambda^2}) \qquad (1)$$

where C is the nuclei concentration. By adjusting the values of ξ and λ, the distribution function (1) can be made to fit most observed nuclei distribution functions. It is preferable to the more frequently used power law because it allows simulation of the peak in the population which is often observed (at $R = \xi$) and of the fact that the population of large bubbles is very small.

The problem is to evaluate how many of these nuclei are convected into the region of low pressure near the minimum pressure point on the surface of the body and therefore grow to observable macroscopic vapor bubbles. Some simplifying observations allow us to avoid lengthy numerical computations of the bubble dynamics (using the Rayleigh-Plesset equation) for every nucleus size, every streamline, every cavitation number, etc.. Meyer *et al.* (1989, 1992) conducted a detailed numerical study of this kind which included most of the effects studied here. In this paper we present a much simpler analytical approach which, though more approximate, is probably as accurate as the current experimental data would merit. Ceccio and Brennen (1992) observed while carrying out numerical integration of the Rayleigh-Plesset equation that, for a given cavitation number, σ, and minimum pressure coefficient, C_{PM}, all nuclei above a certain critical size, $R = R_C$, would grow to roughly the

same observable bubble size and therefore would be registered as "cavitation events". Furthermore, the critical size, R_C, appeared to be almost independent of the details of the pressure/time history and a function only of the difference between the minimum pressure and the vapor pressure (represented non-dimensionally by $(-C_{PM}-\sigma)$), the upstream velocity, U, the fluid density, ρ, and surface tension, S. Specifically,

$$R_C = \frac{8\beta S}{3\rho U^2(-C_{PM}-\sigma)} \qquad (2)$$

fitted the bubble dynamic calculations very well when the empirical parameter $\beta \approx 1$. This expression is, of course, consistent with the stability analyses put forward first by Flynn (1964) and Johnson and Hsieh (1966). Its use does save a great deal of computational effort. Furthermore, it means that we need not concern ourselves with the detailed pressure/time history along the entire length of each streamline but can simply focus on the region around the minimum pressure point.

However, it is necessary to determine how the minimum pressure coefficient, C_{PM}, varies from streamline to streamline. Here again we will use a simple analytic expression derived from much more complex computations. A panel method was developed to solve the potential flow around any axisymmetric headform. This was used to calculate the potential flow around the Schiebe headform. Such calculations suggested that the pressure gradient, dp/dy, normal to the surface in the vicinity of the minimum pressure point could be approximated by $\rho U_M^2/r_K$ where $U_M = U(1-C_{PMS})^{\frac{1}{2}}$ and C_{PMS} are respectively the velocity and pressure coefficient at the minimum pressure point on the surface of the body and r_K is a measure of the radius of curvature of the streamlines in this region. For the Schiebe body (C_{PMS} =-0.78) it is found that r_H/r_K =2.5 provides an approximate representation of the variation in the minimum pressure coefficient, C_{PM}, on a streamline with the distance y of that streamline from the surface. The actual variation of C_{PM} with y from the potential flow calculation is shown in figure 5 along with several approximations. With $dp/dy = \rho U_M^2/r_K$ it follows that

$$C_{PM} = C_{PMS} + 2y(1-C_{PMS})/r_K \qquad (3)$$

This expression allows us to evaluate from equation (2) the critical nuclei size, $R_C(y)$, for each streamline; R_C therefore increases with the distance, y, of the streamline from the surface. A larger critical size means that fewer of the available nuclei will generate cavitation events. The process is terminated on that streamline which just touches the isobar $C_{PM} = -\sigma$ for then the minimum pressure is equal to the vapor pressure and no cavitation events will occur on this streamline or any outside it. Consequently we need

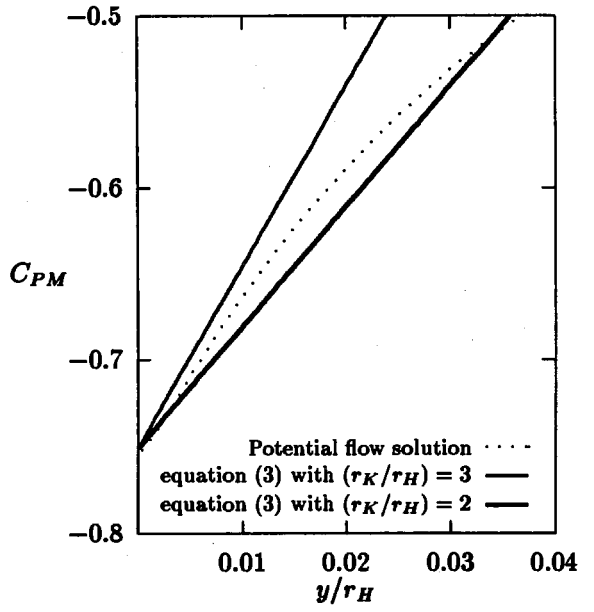

Figure 5: Variation in the minimum pressure coefficient, C_{PM}, on a streamline with the distance y of that streamline from the surface of the body near the minimum pressure point

only be concerned with a region near the surface given by

$$0 < y \leq y_M f_3 \qquad (4)$$

where

$$y_M = \frac{(-C_{PMS}-\sigma)}{2(1-C_{PMS})} r_K \qquad (5)$$

and f_3 =1. Different values of f_3 which is a function of R_M/r_H will be used later to examine the influence of a minimum observable bubble size, R_M. Using the relations (2) and (3) and disregarding any possible effects of the boundary layer or of relative motion between the nucleus and the flow one can then construct an event rate from the nuclei number distribution as follows. The volume flow rate passing through two stream surfaces a distance, dy, apart at the minimum pressure point (see figure 6) is given by

$$2\pi r_S U(1-C_{PMS})^{\frac{1}{2}} f_1(y)dy \qquad (6)$$

where $f_1(y)$ =1, but different values will be used later to account for boundary layer effects. The variable r_S is the radial distance from the axis of symmetry to the minimum pressure point (on the Schiebe body $r_S/r_H \approx 0.75$). It follows from equation (6) that the cavitation event rate in the stream tube, dE, is given by

$$dE = 2\pi r_S U(1-C_{PMS})^{\frac{1}{2}} f_1(y)dy \int_{R_C(y)}^{\infty} \frac{N(R)dR}{f_2(R,y)} \qquad (7)$$

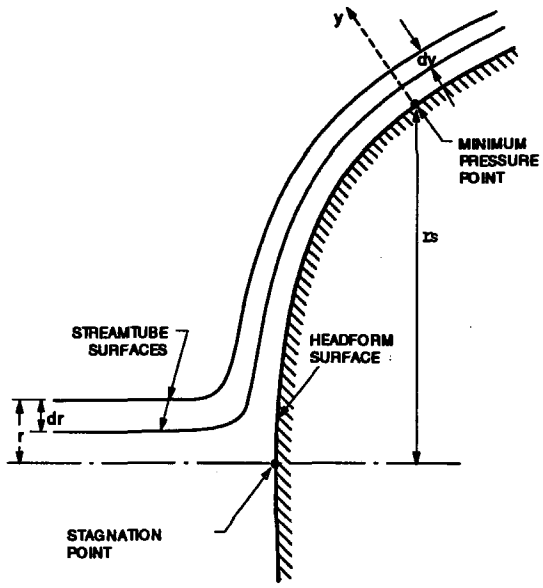

Figure 6: Schematic showing typical annular stream tube upstream and in the neighborhood of the minimum pressure point

where $f_2(R,y)$ =1, but different values will be used later to account for screening effects due to relative motion between the nuclei and the liquid. In the above equation it follows from equations (2) and (3) that

$$R_C(y) = \frac{8\beta S}{3\rho U^2}\left[-\sigma - C_{PMS} - \frac{2y(1-C_{PMS})}{r_K}\right]^{-1} \tag{8}$$

Note that $R_C(y \to y_M) \to \infty$. It follows that the total cavitation event rate, E, will be

$$E = \int_0^{y_M f_3} 2\pi r_S U(1-C_{PMS})^{\frac{1}{2}} f_1(y) \int_{R_C(y)}^{\infty} \frac{N(R)dR}{f_2(R,y)}dy \tag{9}$$

5 Boundary Layer Effect

The above analysis neglected the effects which the presence of a boundary layer might have on the pressure/time history experienced by a potential cavitation nucleus. Several such effects can be envisaged. These include the fact that the boundary layer will reduce the volume flow rate of fluid traveling close to the headform and thus reduce the supply of nuclei. It may also alter the shape of the isobars near the surface. Here we will explore only the first of these two effects. To do so we assume a simple form for the boundary layer profile near the minimum pressure point namely

$$\frac{u}{u_M} = \begin{cases} 2\left(\frac{y}{\delta}\right) - 2\left(\frac{y}{\delta}\right)^3 + \left(\frac{y}{\delta}\right)^4 & \text{for } y < \delta \\ 1 & \text{for } y \geq \delta \end{cases} \tag{10}$$

where δ is the boundary layer thickness. If δ_2 is the momentum thickness, it follows that $\delta_2 = 0.133\delta$ and using the modified Thwaites method to solve for the laminar boundary layer thickness (Thwaites, 1949, Rott and Crabtree, 1952), we find that

$$\frac{\delta_2}{r_H} \approx 0.68\left(\frac{\nu}{r_H U}\right)^{\frac{1}{2}} \tag{11}$$

Then, to account for the decrease in volume flow rate due to the boundary layer, the expressions (6), (7) and (9) should include non unity values for $f_1(y)$ given by

$$f_1(y) = \begin{cases} 2\left(\frac{y}{\delta}\right) - 2\left(\frac{y}{\delta}\right)^3 + \left(\frac{y}{\delta}\right)^4 & \text{for } y < \delta \\ 1 & \text{for } y > \delta \end{cases} \tag{12}$$

with $\delta = 5.10(\nu r_H/U)^{\frac{1}{2}}$.

It is also true that the boundary layer will effect the shape of the isobars and therefore cause some alteration of the expressions (3), (5), and (8); we have not included this effect in the present analysis.

6 Screening Effects

In their study of the potential cavitation of nuclei, Johnson and Hsieh (1966) recognized that the relative motion between the nuclei and the liquid might play an important role in determining the number of nuclei which enter the region in which the pressure is below the vapor pressure. Specifically they recognized that a bubble "screening" effect would occur in which the nuclei are forced away from the body due to the large pressure gradients normal to the streamlines in the vicinity of the stagnation point. This outward displacement would be larger for the larger bubbles. Because one is concerned only with streamlines very close to the stagnation streamline and the body surface and because the streamline curvature and therefore the pressure gradient normal to the streamline is much larger in the vicinity of the stagnation point than anywhere else, we may evaluate this screening effect by focusing attention on the stagnation point flow alone. In order to obtain an estimate of this effect we shall assume that the nuclei under consideration (of radius R) are all sufficiently small that the Reynolds number of the relative motion is much smaller than unity. Then the velocity of the nucleus in a direction normal to the streamline, v, is given by

$$v = \frac{2}{9}\frac{R^2}{\mu}\left(\frac{\partial p}{\partial n}\right) \tag{13}$$

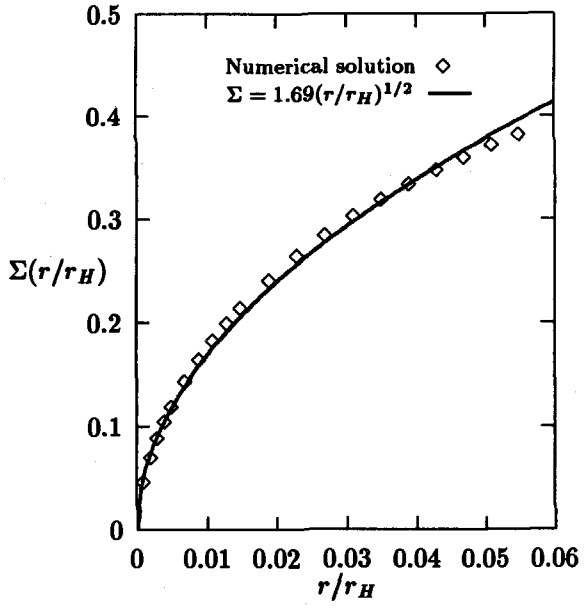

Figure 7: The function $\Sigma(r/r_H)$ for the stagnation point flow in the potential flow around a sphere

where $\partial p/\partial n$ is the local pressure gradient normal to the streamline. Then the total displacement, ϵ, across the streamlines is given by

$$\epsilon = \int_A^B v\, dt = \int_A^B \frac{v}{|q|} ds \tag{14}$$

where $|q|$ is the magnitude of the fluid velocity, the coordinate s is measured along a streamline, A is a point far upstream and B is a location after the large pressure gradients in the vicinity of the stagnation point have been experienced. Note that ϵ will, of course, differ from streamline to streamline and will therefore be a function of r defined as the radial position of the streamline far upstream of the body (see figure 6). Thus

$$\begin{aligned} \frac{\epsilon(r/r_H)}{r_H} &= \frac{2R^2U}{9\nu r_H} \int_A^B \frac{1}{\rho U^2} \frac{\partial p}{\partial (n/r_H)} \frac{U}{|q|}\, d(\frac{s}{r_H}) \\ &= \frac{2R^2U}{9\nu r_H}\, \Sigma(r/r_H) \end{aligned} \tag{15}$$

where $\Sigma(r/r_H)$ is used to denote the dimensionless integral on the previous line.

Since the stagnation point flow is the same on any blunt axisymmetric body it is appropriate to choose to examine the stagnation region in the potential flow around a sphere in order to evaluate $\Sigma(r/r_H)$. This is a non-trivial calculation, and the details will be omitted here for the sake of brevity. The result is the function $\Sigma(r/r_H)$ presented in figure 7; for convenience this can be approximated by the empirical relation

$$\Sigma(r/r_H) = \Gamma(r/r_H)^\gamma \tag{16}$$

where $\Gamma \approx 1.69$, $\gamma \approx 0.5$.

Having evaluated the screening displacement it can be applied to the evaluation of the event rate in the following way. A nucleus of radius R which is on the streamline at radius r far upstream will, when it reaches the low pressure region, be on the streamline which is the following distance, y, from the body surface:

$$\frac{y}{r_H} = \frac{1}{2(1-C_{PMS})^{\frac{1}{2}}} \frac{r^2}{r_S r_H} + \frac{2}{9}(\frac{R}{r_H})^2 \frac{r_H U}{\nu} \Sigma(r/r_H) \tag{17}$$

Thus the stream tube between y and $y+dy$ will contain all the nuclei of radius R which were present in the upstream flow between radii r and $r+dr$ (figure 6) where

$$\frac{dy}{r_H} = \frac{r\, dr}{(1-C_{PMS})^{\frac{1}{2}} r_S r_H} f_2(R,y) \tag{18}$$

and

$$f_2(R,y) = 1 + \frac{2}{9}(\frac{R}{r_H})^2 (\frac{r_H U}{\nu})(1-C_{PMS})^{\frac{1}{2}} (\frac{r_S}{r_H}) \frac{r_H}{r} \Sigma' \tag{19}$$

where Σ' denotes $d\Sigma/d(r/r_H)$ and r and y are related by equation (17). Since the liquid flow between y and $y+dy$ is still given by the expression (6), it follows that the actual number distribution function for the stream tube between y and $y+dy$ is $N_E(R,y)$ where

$$N_E(R,y) = N(R)/f_2(R,y) \tag{20}$$

Consequently the screening effect alters the event rate by introducing a non-unity expression for $f_2(R,y)$ in the expression (9), namely that given by equation (19).

7 Observable cavitation bubble size effect

Normally, experimental observation can only detect cavitating bubbles when they achieve a certain observable size, say R_M, and in this section we shall incorporate this "observable cavitation bubble size effect" in our analysis. This requires an analysis of the maximum size, R_{max}, achieved by the cavitation bubble. To do so we represent the pressure coefficient near the minimum pressure point approximately by

$$\begin{aligned} C_P &= C_{PMS} + \frac{2y(1-C_{PMS})}{r_K} + \frac{C_{P1}^* |s-s_0|}{r_H} \\ &= C_{PM} + \frac{C_{P1}^* |s-s_0|}{r_H} \end{aligned} \tag{21}$$